



High-resolution mapping of the mantle transition zone and its interaction with subducted slabs in the Ibero-Maghrebian region

J.A. Parera-Portell ^{a,b,*}, F.d.L. Mancilla ^{a,b}, J. Morales ^{a,b}, J. Díaz ^c

^a Instituto Andaluz de Geofísica, Universidad de Granada, c/Prof. Clavera n.12, Granada, 18071, Spain

^b Departamento de Física Teórica y del Cosmos, Universidad de Granada, Campus de Fuente Nueva, Granada, 18071, Spain

^c Geosciences Barcelona, CSIC, c/Lluís Solé i Sabarís s/n, Barcelona, 08028, Spain

ARTICLE INFO

Editor: H. Thybo

Keywords:

receiver functions
Iberia
NW Africa
mantle transition zone
subduction

ABSTRACT

The mantle transition zone (MTZ) beneath Iberia and NW Maghreb has been precisely mapped using more than 56000 high-quality P-wave receiver functions calculated from the data collected by permanent seismic networks and multiple temporary deployments in the region. Three-dimensional depth migration using both regional and global tomographic models has allowed us to obtain robust and continuous measurements of the MTZ thickness and the depth of the 410 and 660 discontinuities. We found the MTZ thickened by as much as 30 km in the Mediterranean coast due to the effect of the cold Gibraltar-Alboran and Alpine-Tethys slabs. Coinciding with expected water-enriched MTZ areas near the subducted slabs there is evidence for partial melting atop the 410 in at least three low-velocity layers (LVL). Partial melting is also likely in a LVL in the uppermost lower mantle under the Alpine-Tethys slab, while we attribute other intra-MTZ LVL to increased mineralogical heterogeneity. We link a thinning of the MTZ at the rear of the Gibraltar-Alboran slab to mantle upwelling, and a band of depressed 410 along its southern boundary as an area of hot toroidal flow. A discontinuous region of depressed 410 following the Atlas Mountains also supports mantle upwelling beneath this range. Areas with LVL atop a depressed 410 discontinuity correlate well with active intraplate volcanism, suggesting a possible MTZ source. We also found that deep-focus seismicity occurs where the 660 discontinuity starts to deepen at the westernmost edge of the Gibraltar-Alboran slab.

1. Introduction

The Western Mediterranean has undergone a complex tectonic evolution during the Cenozoic. The roughly N-S Nubia-Eurasia convergence led to the consumption of the ancient Alpine-Tethys Jurassic oceanic lithosphere through a subduction zone that eventually split into multiple slabs, all migrating in different directions: W (Gibraltar-Alboran slab), S (Algerian slab) and E (Apennines-Calabria slabs) (e.g. Spakman and Wortel, 2004; Faccenna et al., 2014). The retreat of the Gibraltar-Alboran trench caused the westwards displacement of a highly arcuate deformation front (the Gibraltar arc), leading at the same time to extensional tectonics at its rear and the subsequent opening of the Alboran Basin (e.g. Faccenna et al., 2004). Nowadays the forearc extends well into the Gulf of Cadiz in the Atlantic, but subduction appears to have ceased or, at any rate, to have greatly slowed down (e.g. Stich et al., 2006; Diaz et al., 2021). The subduction history of the Western Mediterranean means that several pieces oceanic lithosphere remain in the

Earth's mantle, introducing temperature anomalies and chemical heterogeneity. Locating and accurately delineating these anomalies may shed light both on the present and past evolution of the region.

The mantle transition zone (MTZ) discontinuities, namely the 410 and 660 as they occur globally at these average depths, are sensitive to changes in the mantle's thermal state and thus are good proxy indicators of anomalies such as cold subducted slabs or hot mantle plumes. Consensus is that both discontinuities are caused by olivine phase transitions in a pyrolitic mantle: olivine (Ol) to wadsleyite (Wd) at 410 km and ringwoodite (Rw) to bridgmanite (Br) and magnesiowüstite (Mw) at 660 km. The Clapeyron slope of the Ol-Wd transition is positive whereas it is negative in the Rw-Br case, resulting in discontinuities that show the opposite response for a same temperature variation: a cold anomaly makes the 410 shallower and the 660 deeper, while a hot anomaly causes the contrary effect. The thickness of the MTZ is therefore also dependent on the thermal state of the mantle, thickening when colder and thinning when hotter (e.g. Collier and Helffrich, 1997; Schmerr and

* Corresponding author.

E-mail address: jpareraportell@ugr.es (J.A. Parera-Portell).

<https://doi.org/10.1016/j.epsl.2024.118798>

Received 29 December 2023; Received in revised form 10 May 2024; Accepted 20 May 2024

Available online 30 May 2024

0012-821X/© 2024 The Author(s). Published by Elsevier B.V. This is an open access article under the CC BY license (<http://creativecommons.org/licenses/by/4.0/>).

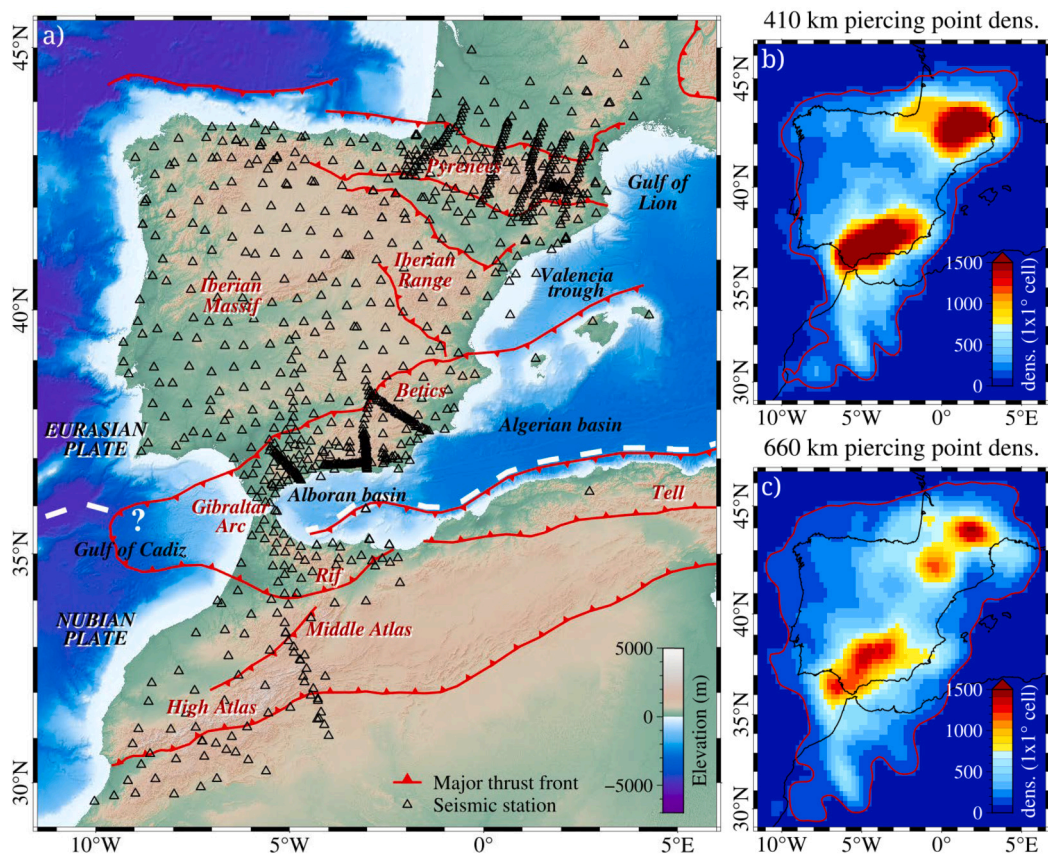


Fig. 1. a) Tectonic setting and location of the seismic stations, (see Acknowledgments section and Supplementary Information for network names and references). Red fronts mark the limits of the major tectonic units in the region, adapted and simplified from previous works (e.g. Serpelloni et al., 2007; Civiero et al., 2018). A dashed white line marks the boundary between the Eurasian and Nubian plates. b) and c) show the density of piercing points and the minimum density boundary (red line) at the depths of the MTZ discontinuities. The red line contains the final area of interest, with a minimum density of 100 piercing points in 1° radius. All maps are in Mercator projection.

Garnero, 2007, and references therein). Still, the 410 and 660 are not only sensitive to temperature, but also to chemical heterogeneity. Water is frequent around subducted slabs due to dehydration reactions, and may cause the 410 to become shallower and thicker and the 660 deeper and sharper (Litasov and Ohtani, 2007). The composition of Ol in the upper mantle also affects the Ol-Wd transition, which becomes deeper if the Ol is Fe-poor (e.g. Schmerr and Garnero, 2007). Other phase changes may appear near MTZ depths, such as majorite (Mj) to perovskite (Pv). Mj-Pv has a positive Clapeyron slope and becomes the dominant transition at the base of the MTZ when temperatures exceed 2100 K, so the 410 and 660 discontinuities can display the same behavior where the MTZ is hottest (e.g. Sun et al., 2017; Waszek et al., 2021).

In this study we use P-to-S wave conversions at the MTZ discontinuities to map the 410 and 660 topography in the Ibero-Maghrebian region. To achieve this we take advantage of P-wave receiver function analysis, a seismic technique capable of obtaining time series of P-to-S wave conversions from teleseismic three-component records. Our dataset is the largest used in this region to date, which brings the opportunity to obtain continuous high-resolution maps of the anomalies in the MTZ and expand on previous analyses by Bonatto et al. (2015).

2. Data and methods

Our dataset comprises 881 broadband three-component seismic stations from 13 permanent networks and 18 temporary deployments located in NW Africa, the Iberian Peninsula and southern France (Fig. 1, see Supplementary Information for references).

P-wave receiver function analysis (Vinnik, 1977; Langston, 1979) is a method that allows the detection of seismic discontinuities through P-to-S wave conversions that occur whenever a seismic wave reaches a velocity contrast. Receiver functions are time series containing such wave conversions, and can be regarded as the impulse response of the medium. Isolating conversions within seismic records is possible with three-component seismometers by deconvolving the vertical from the horizontal components, eliminating redundant information and keeping only the response of the near-receiver structure. Ideally, in a flat and horizontal medium all the energy of the receiver functions should be contained in the P-SV wave plane, SV being vertically polarized S-waves.

For receiver function analysis, teleseismic events (distance of 30° to 90°) of magnitude ≥ 6 were selected, keeping the P-wave arrival and its coda. The waveforms were detrended, filtered (high-pass, 0.5 Hz corner frequency) and finally decimated to 10 Hz. An initial selection of events was made based on the signal to noise ratio, keeping only waveforms with a ratio above 2. To approximate the P-SV plane the ZNE components were rotated to LQT with each event's backazimuth and the theoretical incidence angle at the receiver. This rotation isolates most P-wave energy in the L components and wave conversions in the Q components. Still, given that the incidence angle is theoretical and that there may be anisotropy or dipping discontinuities underneath the stations, we expect some SV energy to leak into the T components. Receiver functions were calculated with the iterative time domain deconvolution method (Ligorría and Ammon, 1999), using a Gaussian width factor of 0.5. A second automatic quality control was done after receiver function calculation, based on the individual root-mean-square error (RMSE) and the median absolute deviation (MAD) at each seis-

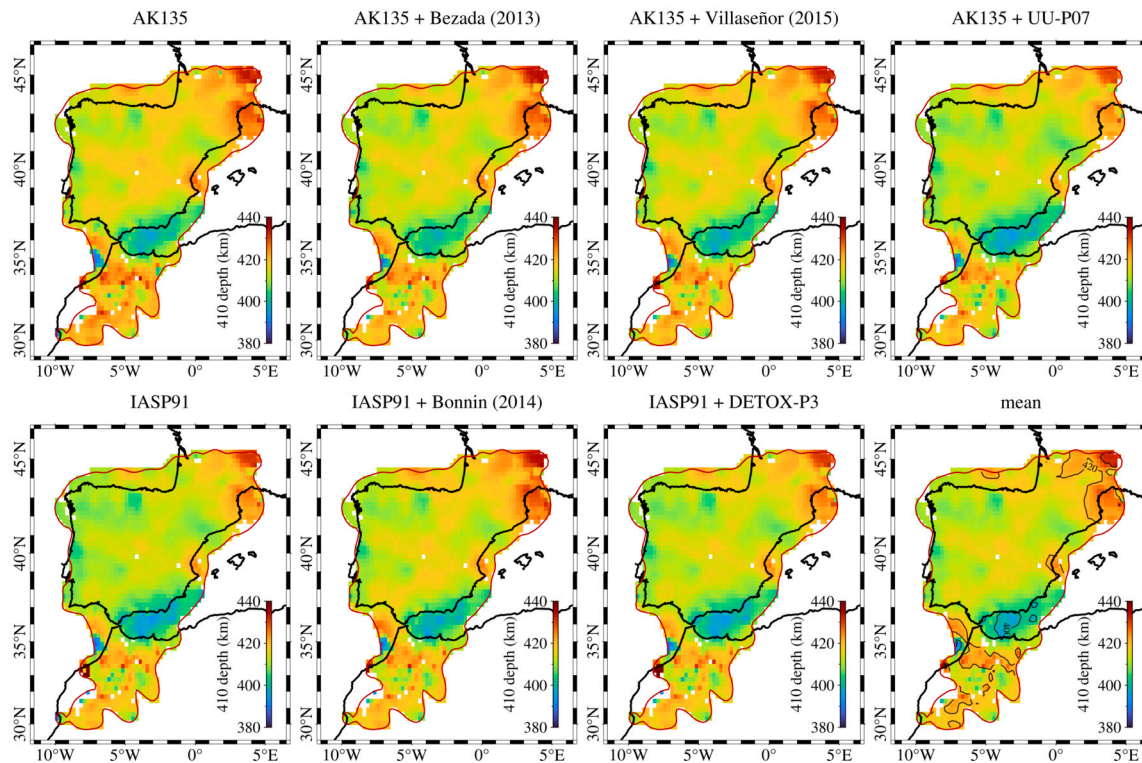


Fig. 2. 410 discontinuity depth according to the different 1D reference earth models and P-wave tomography models. The map in the lower right shows the average 410 depth of 3D migrations and features ± 10 km and ± 20 km anomaly contour lines. The limit of the study area is shown in red.

mic station. We only kept receiver functions with RMSE below 30 % (i.e. those that can recover at least 70 % of the original waveforms) and with a maximum amplitude of 5 MAD. The MAD test is only used to remove data affected by spurious high-amplitude signal resulting from anomalies in the original waveforms. We finally obtained 56528 high quality receiver functions.

The final areas of interest for the 410 and 660 discontinuities were selected according to the density of piercing points at 410 km and 660 km in a 1° radius. The minimum density threshold was set at 100 piercing points, providing a unique high density spatial sampling of the MTZ. As ray paths spread as they travel downwards, the maximum density is lower at 660 km than at 410 km, but sampling is also more homogeneous. Density is highest in both cases in the Pyrenees and the Betic System due to the denser station deployments (see Fig. 1).

To image the MTZ we used the common-conversion point (CCP) stacking method (e.g. Yuan et al., 2000). This stacking technique consists in backprojecting receiver functions and stacking its amplitudes along a predefined 2D distance-depth grid. Data were stacked according to the first Fresnel zone at each depth, and the phase weighting technique in Frassetto et al. (2010) was employed to prevent the stacking of noise. N-S and E-W CCP profiles at 0.25° intervals were obtained, from 46.50N to 29.00N and from 11.00W to 6.50E . The lateral sampling at each side of the profiles was set at 50 km to allow superposition. As we anticipate a highly heterogeneous mantle with laterally varying seismic velocities, we did not rely on a single 1D reference earth model, as this could lead to bias in the 410 and 660 discontinuity depths. Thus, for each N-S and E-W profiles seven different CCP stacks were calculated. Two CCP were obtained using the IASP91 and AK135 1D reference models with no additional input. For the remaining five CCP stacks the reference models were combined with regional (Bezada et al. (2013), Bonnin et al. (2014) and Villaseñor et al. (2015)) and global (DETOX-P3 (Hosseini et al., 2019) and UU-P07 (Amaru, 2007)) P-wave tomography models. When backprojecting receiver functions along a profile the corresponding 1D reference model was then updated with the P-wave anomaly at any given pair of coordinates and depth. S-wave

velocities were set according to a fixed V_p/V_s ratio of 1.81, a value chosen to be close to mean upper mantle V_p/V_s in the 1D reference models. S-wave tomography was not used because the models either did not have enough resolution to image the slabs in the area or used different reference models than the selected P-wave tomographies.

From the CCP profiles we obtained 410 and 660 depth by searching for the most prominent pulse within a given range of depths and selecting its maximum as the discontinuity location. Then, maps of 410 and 660 depth and MTZ thickness (with a cell size of 0.25°) were obtained with inverse distance weighting interpolation (e.g. Mitás and Mitásova, 1999), while keeping gaps with no data. The temperature anomalies corresponding to the largest depth changes were estimated using the Clapeyron slopes in Tauzin and Ricard (2014): 2.8 MPa K^{-1} for the 410 (Ol-Wd transition) and -3.1 MPa K^{-1} for the 660 (Rw-Br). Note that chemical heterogeneity was not accounted for and therefore the thermal anomalies are probably an overestimation.

3. Results and discussion

The spatial distribution of receiver functions and their piercing points at 410 km and 660 km, although uneven (Fig. 1), allowed for a continuous and high resolution imaging of both the 410 (Fig. 2) and 660 (Fig. 3) discontinuities within the selected boundaries. While a few places remain where no discontinuity was detected, these are not constrained to the areas with poorer data coverage. Most gaps, especially those that are not found along the study area boundaries, are thus to be interpreted as regions where the discontinuities become faint enough not to be detected. Those gaps eventually propagate to the MTZ thickness maps (Fig. 4), which are also constrained by the smaller analysis area of the 440 discontinuity.

The effect of including 3D P-wave velocity anomalies in the depth migration is clearly seen both in the discontinuity depths (Figs. 2 and 3) and in the MTZ thickness maps (Fig. 4). Even though all features remain visible disregarding the reference model or tomography used, the 1D migration generally results in a shallower 660 discontinuity and a

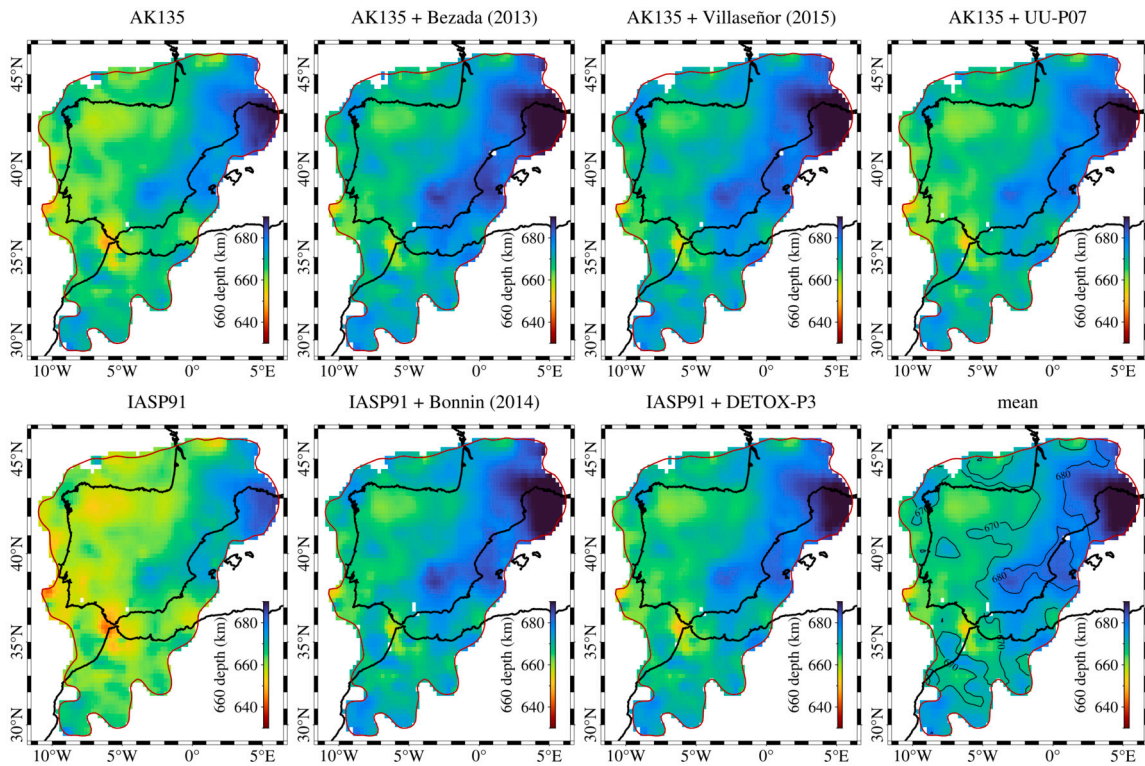


Fig. 3. 660 discontinuity depth according to the different 1D reference earth models and P-wave tomography models. The map in the lower right shows the average 660 depth of 3D migrations and features ± 10 km and ± 20 km anomaly contour lines. The limit of the study area is shown in red.

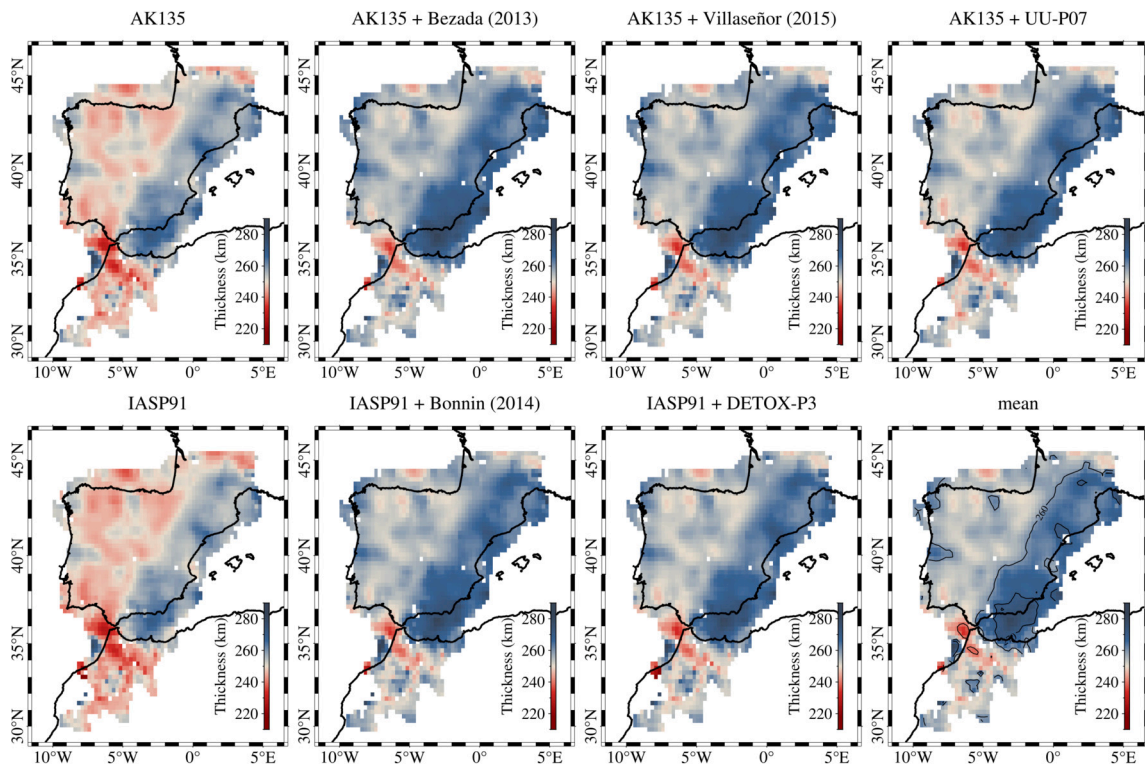


Fig. 4. Mantle transition zone thickness according to the different 1D reference earth models and P-wave tomography models. The map in the lower right shows the average thickness of 3D migrations and features ± 10 km and ± 20 km anomaly contour lines.

thinner MTZ. It is also worth noting that 3D migrations result in remarkably similar maps no matter the selected tomographic model. This provides support to the interpretations of the absolute depth variations of the 410 and 660 discontinuities. Uncertainty was assessed by boot-

strapping the 660 depth measurements at six $1^\circ \times 1^\circ$ cells with prominent 660 pulses (200 iterations). The 660 discontinuity was chosen because the uncertainty is expected to be larger due to the greater seismic velocities. The average uncertainty, given as two standard deviations, was

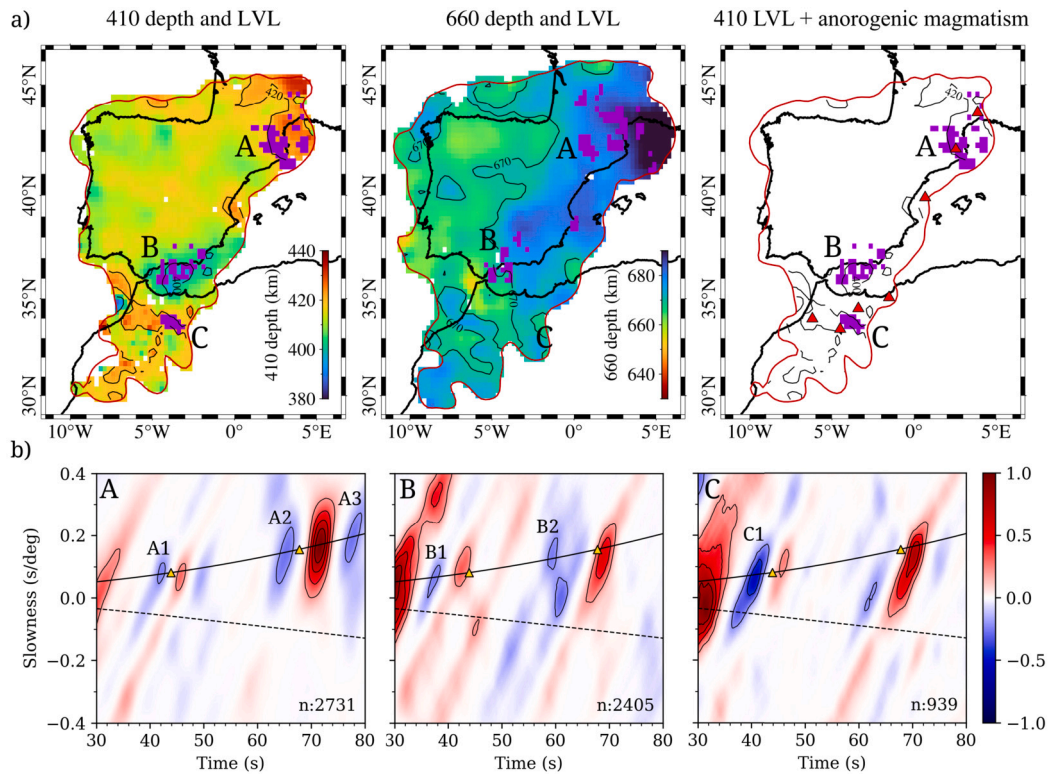


Fig. 5. a) Zones where LVL (purple) were detected on top of the 410 (left) and 660 (middle), alongside the location of active anorogenic volcanism (right, red triangles, Carminati et al., 2012). LVL were automatically detected with the same pulse-search algorithm used for the 410 and 660, but only clusters with unambiguous conversions (A, B and C) in the slant stacks were kept. Contour lines are shown for ± 10 km anomalies and the study area limits are shown in red. b) Slant stacks of the A, B and C clusters (normalized amplitude). Wave conversions follow the upper solid line, while multiples appear along the lower dashed line. The theoretical arrival times of P410s and P660s according to the AK135 reference model are shown as yellow triangles. N is the number of receiver functions in each stack.

estimated at 8.5 km, which is smaller than the inherent uncertainty of the receiver functions. For a Gaussian width parameter of 0.5 a pulse width of ~ 2.35 s is expected, meaning that the minimum depth change that S-waves at 410 km and 660 km can resolve is ~ 11 km and ~ 13 km respectively. Therefore, even though stacking leads to coherent pulses which tend to converge at the real discontinuity depth, we restrict our discussion to areas where the anomaly is at least ± 10 km. In the following analysis all depths are taken from the 3D migration average maps for the sake of robustness. Major MTZ anomalies in our study area occur in the Gibraltar-Alboran Sea area and along the Mediterranean coast of Iberia: the MTZ is considerably thicker than usual in the Alboran Sea, the eastern Betics and around the Gulf of Lion, while beneath the Strait of Gibraltar and the southern border of the Rif it becomes remarkably thin (Fig. 4). The Iberian Massif and the Atlas have a thickness generally close to the standard 250 km, although anomalies in the individual discontinuities may still be present. The 410 discontinuity is near-standard beneath most of Iberia, with local anomalies clustering in NW Maghreb, the Gulf of Cadiz and the Mediterranean coasts. In NE Iberia, the Alboran Sea and the Rif-Middle Atlas contact the major 410 anomalies are accompanied by a shallower negative pulse indicating the presence of low-velocity layers (LVL) (Fig. 5a). Even though these pulses are rather discontinuous, they are consistently imaged in the CCP profiles and show clear converted wave signatures in the slant stacks (Fig. 5b). We label these discontinuities as A1 (NE Iberia, 330-370 km depth), B1 (Alboran Sea, 330-400 km depth) and C1 (Rif-Middle Atlas, 380-390 km depth). In NE Iberia and the Alboran Sea there are additional LVL on top of the 660 (A2 at 580-660 km depth and B2 at 570-610 km depth), and another clear negative conversion is found directly below the 660 beneath the Gulf of Lion (A3, 745-760 km depth). Other negative pulses occur locally outside these three regions around the 410 and 660 dis-

continuities, but these are either clearly identified as multiples or the slant stacks remain inconclusive.

The thickening of the MTZ both in NE and SE Iberia is consistent with anomalies imaged in existing tomographic models (Fig. 6a): in NE Iberia the models see a stagnant chunk of oceanic lithosphere, a remnant of the Alpine-Tethys slab (Spakman and Wortel, 2004), lying on top of the 660 discontinuity and thus not directly affecting the 410, while in SE Iberia the MTZ is affected by the cold oceanic lithosphere of the Gibraltar-Alboran slab sinking almost vertically. In the following sections we discuss the MTZ anomalies region-wise: 1) NE Iberia and Gulf of Lion, 2) S Iberia and Alboran Sea and 3) NW Maghreb.

3.1. NE Iberia and Gulf of Lion

In NE Iberia and the Gulf of Lion, the thickening of the MTZ is exclusively due to a deeper than usual 660 discontinuity. There, the 660 reaches the deepest point in the study area at ~ 693 km, that is, a depth anomaly of 33 km. Neglecting the effect of chemical heterogeneities, this yields a thermal anomaly of -418 K. The 410 is not anti-correlated and instead deepens as much as 22 km in the top NE, which corresponds to a 272 K anomaly. Still, the 410 depression is not large enough to counteract the deepening of the 660, leaving a MTZ that is at least 10 km above its standard thickness. The geometry of the Alpine-Tethys remnant on top of the 660 discontinuity beneath NE Iberia is relatively simple: as the cold chunk of ancient oceanic lithosphere sinks sub-horizontally (e.g. UU-P07 model, Amaru, 2007), it pushes the 660 discontinuity downwards and increases its sharpness (see Fig. 5b, stack A), but it does not directly affect the 410 (Fig. 7). Accompanying the 410 depression is LVL A1 (Fig. 5, zone A), which was previously detected by Bonatto et al. (2015) and matches remarkably well the areas where the 410 anomaly exceeds -10 km. LVL A2, on top of the 660,

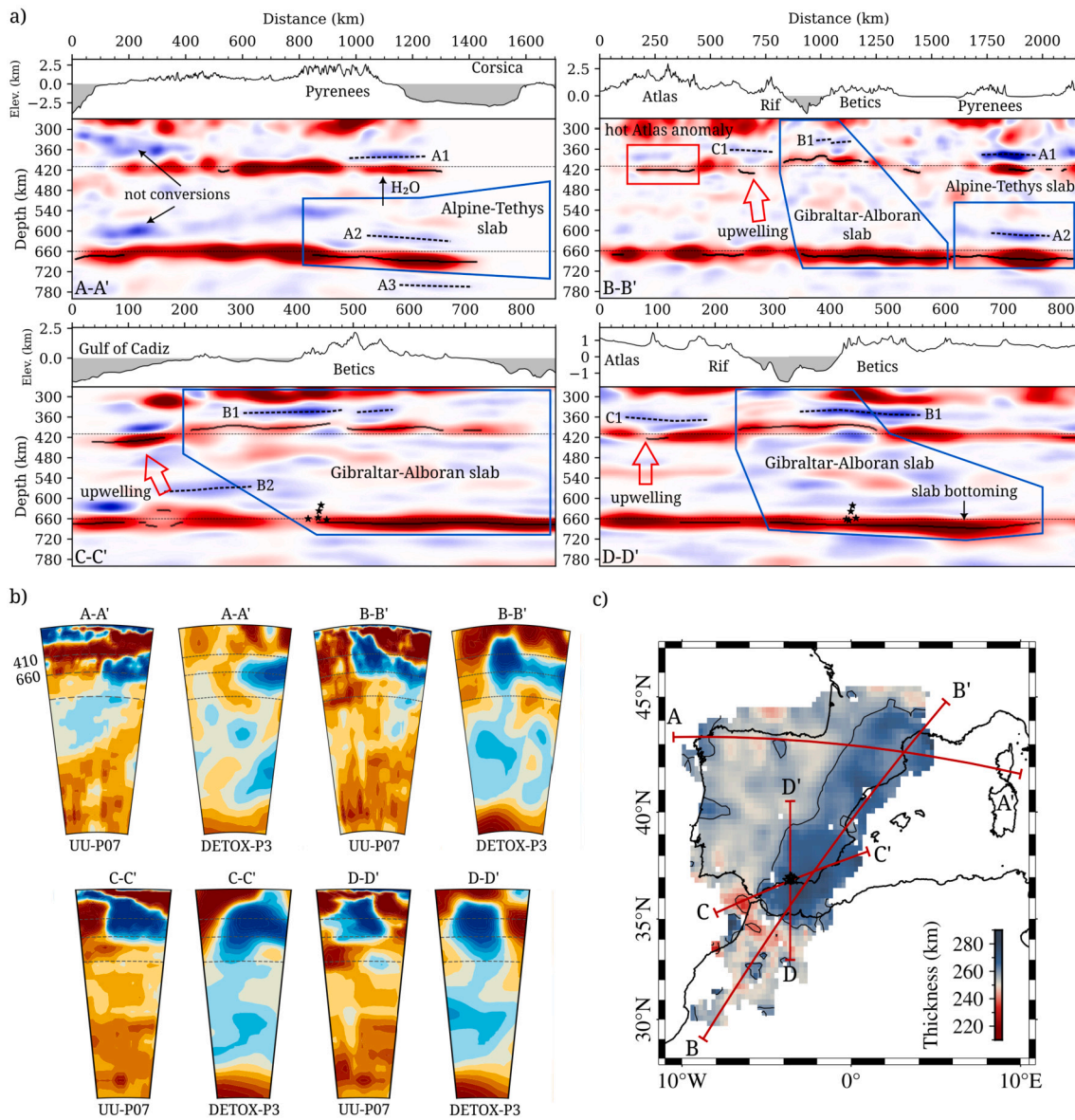


Fig. 6. a) Interpreted CCP cross-sections (blue and red for negative and positive polarity, respectively). A solid black line indicates discontinuity anomalies greater than ± 10 km. Hypocenters of deep-focus earthquakes are shown as black stars. b) Cross-sections of tomographic models UU-P07 and DETOX-P3 from SubMachine (Hosseini et al., 2018) (blue and red for high and low P-wave velocity anomalies, respectively). The scale ranges from -1% to 1% dVp. c) Location of the cross-sections (bars at each end of the profiles indicate the lateral sampling).

has a greater extension but seems more discontinuous. A3 is restricted to the Gulf of Lion matching the areas with the deepest 660, but we can not determine if it extends further to the E. Analogous LVL are found in Western North America associated to the stagnant Farallon slab (e.g. Tauzin et al., 2013, 2017) and in NE China above stagnant portions of the subducted Pacific plate (e.g. Schmandt et al., 2014; Tauzin et al., 2017; Han et al., 2021). In light of this, we contemplate a similar origin for these discontinuities in NE Iberia.

LVL A1 occurs above the stagnant Alpine-Tethys lithosphere and is likely caused by slab dehydration. Taking into account global models of downgoing water flux in subduction zones (e.g. van Keken et al., 2011), we believe that it is feasible for at least some water fraction to have been carried to the base of the MTZ. A comparison through the thermal parameter (Φ , the product of slab age and convergence rate) can be made with the neighboring Calabria ($\Phi = 8550$) and Aegean ($\Phi = 3000$) slabs, with a water flux at 230 km depth of $8.0-8.9 \text{ Tg Myr}^{-1} \text{ m}^{-1}$ and $0.5 \text{ Tg Myr}^{-1} \text{ m}^{-1}$, respectively (van Keken et al., 2011). Given the old age of the Alpine-Tethys slab and its past average subduction rate

of $20-30 \text{ mm yr}^{-1}$ (Faccenna et al., 2014), we estimate Φ at 4000-6000, placing the water flux somewhere in between the Calabria and Aegean cases. Moreover, in such cold subduction zones dehydration past 230 km is minor (van Keken et al., 2011). Therefore, we speculate that the Alpine-Tethys slab can release water in the MTZ and hydrate the surrounding Wd, which becomes buoyant, rises and transitions to Ol at the 410 discontinuity. Ol can hold less water in its structure than Wd so the mantle on top of the 410 becomes saturated, leading to partial melting and a decrease of seismic velocities (e.g. Bercovici et al., 2003; Leahy and Bercovici, 2007; Freitas et al., 2017). Increased water content near the 410 should result in an upwards deflection of the discontinuity (e.g. Litasov et al., 2005), but instead we encounter A1 in areas where the 410 is significantly depressed. A hotter mantle temperature, maybe due to the rising of hot hydrated Wd, in combination with Fe depletion caused by partial melting could counteract the effect of water and deflect the 410 downwards (e.g. Schmerr and Garnero, 2007) without the need for a 120-272 K temperature increase.

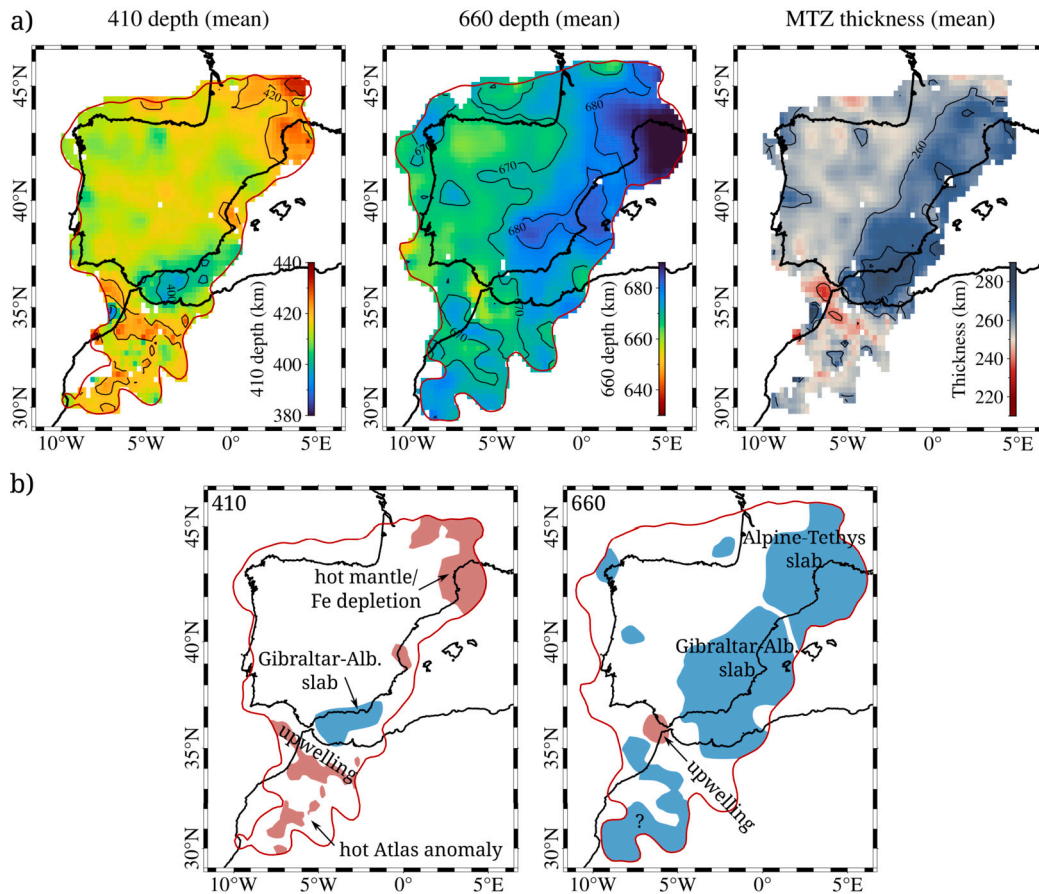


Fig. 7. a) Averaged 410 depth, 660 depth and MTZ thickness maps (from 3D migration results only). Contour lines are shown for ± 10 km anomalies. b) Interpretation for 410 (left) and 660 (right) anomalies (blue and red for cold and hot anomalies, respectively).

Atop the 660 discontinuity, LVL A2 is likely linked to intra-slab chemical heterogeneities. Stratification involving the detachment of denser basaltic crust from the top of the slab, the presence of a Mg garnet layer of lower velocity than the surrounding mantle or an excess of water could all explain a velocity reduction at the base of the MTZ (Touzain et al., 2013; Wang et al., 2020; Shen et al., 2014). Water is also probably increasing the velocity contrast at the 660 discontinuity (Shen et al., 2014, and references therein), which achieves the largest conversion amplitude in the study area (see 660 conversion in Fig. 5b, stack A). LVL A3 appears to be caused by the hydration and partial melting of Br at the top of the lower mantle (e.g. Schmandt et al., 2014), as it is more localized and occurs only where the Alpine-Tethys slab is bottoming. Overall, observations support that the Alpine-Tethys slab is still hydrated to some extent.

3.2. S Iberia and Alboran Sea

The 410 and 660 discontinuities below S Iberia and the Alboran Sea are anti-correlated and leave a MTZ with a maximum thickening of 30 km. The 410 is uplifted up to 16 km and the 660 is depressed by as much as 24 km. If we consider only the effect of temperature, these depth changes translate to thermal anomalies of -198 K in the 410 and -304 K in the 660. The largest anomalies are however not on top of each other, so while the 410 anomaly is mainly restricted within the Alboran Sea, the deepest 660 is found about 200 km further to the N. The Gibraltar-Alboran slab is still attached to the lithosphere in sections of the western Betics and the Rif, dipping E almost vertically (e.g. Bezada et al., 2013; Civiero et al., 2020). However, the slab bends from a N-S direction to roughly W-E along the SE coast Iberia. In this section the slab is detached from the lithosphere through

a Subduction-Transform-Edge-Propagator (STEP) fault (Mancilla et al., 2018) and dips also almost vertically to the S-SW. The geometry seen in the 410 depth maps (Fig. 2) reflects this N-S to W-E direction change with the -10 km anomaly occupies the Alboran Sea and extends into the Algerian Basin along the SE coast of the Iberian Peninsula. The 410 is locally hard to detect in this area as the conversions may become faint, leading to some gaps beneath the Rif. Even though the Gibraltar-Alboran slab dips almost vertically until it reaches the 410, the 660 anomaly in Fig. 3 indicates that the W-E detached slab section bends at depth and starts dipping to the N, leaving the maximum 660 anomaly displaced towards the center of Iberia (Fig. 7). The overturning of the Gibraltar-Alboran slab at MTZ depths is supported by waveform analysis (Sun and Miller, 2024) and may be analogous to previously reported slab overturning beneath the Alps (Handy et al., 2021).

LVL B1 is found in the northern half of the Alboran Sea, and correlates with the maximum 410 anomaly (Fig. 5a, zone B). The depth and location of this LVL point at a case of dehydration melting as the Gibraltar-Alboran slab reaches the MTZ. On the contrary B2 occurs mostly outside the areas with depressed 660, further to the W. Unlike LVL A2, B2 appears not to be an intra-slab discontinuity and is on top of an unusually wide 660 (up to 40 km of full-width at half maximum) which further into the Gulf of Cadiz evolves into a lenticular geometry that is indicative of multiple phase changes (Fig. 6b, profile C-C'). The significantly depressed 410 in the Gulf of Cadiz, the overall thinning of the MTZ and the low velocities imaged in this region (Fig. 6a, tomography profile C-C') provide evidence for a hot mantle upwelling occurring at the back of the Gibraltar-Alboran slab. LVL have been found to occur in the lower MTZ at sites of mantle upwelling, related to the rising of mantle assemblages enriched in low velocity Mj (Nagel et al., 2018). We believe that B2 is a case of Mj-related LVL, and that as previously

suggested in Bonatto et al. (2015) the double 660 under the Strait of Gibraltar consists of a shallower Rw-Br and a deeper Mj-Pv phase transition. From the deepening of the 410 in this area we expect a positive thermal anomaly of ~ 185 K.

3.3. NW Maghreb

Along the western and southern edges of the Gibraltar-Alboran slab the 410 deepens significantly in an arc stretching from the Gulf of Cadiz to the Rif-Middle Atlas tectonic contact (Fig. 2). We speculate that shallower local upwellings and a toroidal flow from the back of the Gibraltar-Alboran slab towards the Alboran Sea are deepening the 410 here, in agreement with the rollback motion of the slab and SKS splitting measurements (Diaz et al., 2010). The 410 deepens as well in the High and Middle Atlas in a discontinuous manner. Overall, 410 anomalies in the region are typically within a 10 km-15 km range, or equivalently ~ 120 K to ~ 185 K, but very locally reach 18 km (~ 222 K). Low velocity anomalies in the MTZ and the upper mantle are widespread under the Atlas according to the tomography models (Fig. 6a, profile B-B') and upwelling is thought to be a major mechanism behind the uplift of the range (Miller and Becker, 2013), explaining well the deeper 410. However, we found no evidence for hot plumes going from the base of the MTZ to the upper mantle: the 660 discontinuity shows a subtle and discontinuous deepening (barely exceeding 10 km) and never rises significantly above its standard depth nor features a second pulse attributable to the Mj-Pv transition. We also found no significant anti-correlation (or correlation) between the 410 and 660 discontinuities in the area, so there is no evidence for plumes even if Mj-Pv is considered the dominant transition, which would require very high temperatures at the base of the MTZ. Overall, the lack of correlation renders a MTZ thickness that does not deviate much from the standard 250 km (Fig. 7).

The LVL C1 is located at the Rif-Middle Atlas contact directly S of the Alboran Basin, and is the most prominent of the LVL in the slant stacks (Fig. 5b, zone C). C1 coincides with the intersection of the bands of depressed 410 associated to the hot Atlas mantle region and the upwelling and mantle flow W and S of the Gibraltar-Alboran slab. Upwelling here in the Middle Atlas is supported by a number of previous studies (Sun et al., 2014; Civiero et al., 2019; Lee et al., 2022) and the regional thermal anomalies, even if considering anisotropy, allow for the presence of melts in the upper mantle when considering a water-rich environment (Lee et al., 2022). Being near the subducted Gibraltar-Alboran slab we guess that the MTZ in this area has an increased water content, favoring partial melting at LVL C1 as the hydrated Wd transitions to water-saturated Ol.

3.4. Remarks on the active anorogenic magmatism and deep-focus seismicity

Remarkably, active anorogenic magmatism in the western Mediterranean clusters on top or near regions of depressed 410 (Fig. 5a). In NE Iberia, SE France and the Rif-Middle Atlas the presence of partial melts atop the 410 discontinuity raises the question of whether anorogenic magmatism could be related, at least partially, to a hydrous MTZ as is the case in NE China (Yang and Faccenda, 2020). This hypothesis seems most likely in the Middle Atlas, where Sun et al. (2014) imaged an upwelling conduit in the upper mantle that they link to the magmatism in the area. This conduit correlates well with LVL C1 and suggests a possible MTZ source for the melts.

Another noteworthy feature of the Ibero-Maghrebian region is the deep-focus seismicity found under Granada, still of unknown origin. The earthquakes occur close to the 660 discontinuity, in an area already deepened slightly by the action of the cold Gibraltar-Alboran slab (Fig. 6). The hypocenters do not coincide with the region with largest 660 anomaly, but instead lie close to the lower western edge of the slab. Immediately to the W of the hypocenters a region with no 660 detection appears, after which the 660 rises up to its standard depth. There

is also a rapid transition towards a standard 660 to the SW. In this scenario a high W-E temperature gradient is expected given the hot mantle anomaly behind the slab, as already noted in Bonatto et al. (2015). Also, it is in this region that the Gibraltar-Alboran slab starts pushing the 660 discontinuity downwards. Although it is beyond the scope of this study to find the mechanism driving deep-focus seismicity, we highlight that the deep earthquakes beneath Granada occur under very specific conditions, that is: a) in an area of high temperature gradient, b) near the borders of the slab with possibly some remaining water content and c) where the 660 starts to deflect downwards as a response to slab rollback.

4. Conclusions

The high-resolution mapping of the 410 and 660 discontinuities revealed both large and small-scale anomalies in the MTZ (Fig. 7). Cold thermal anomalies corresponding to the Gibraltar and Alpine-Tethys slab dominate the MTZ thickness pattern in the region, but our results prove that chemical heterogeneities are also significant. Water released by the slabs is a key factor, as a water-enriched MTZ is required to explain partial melting atop the 410 discontinuity and the increased 660 sharpness where the Alpine-Tethys slab is bottoming. As water causes the same topography variations on the 410 and 660 than a cold anomaly, the thermal anomalies that we predict from the corresponding Clapeyron slopes are most probably overestimated.

Upwelling occurs at the back of the Gibraltar-Alboran slab, and there we also see both the effects of thermal and chemical anomalies. A significant amount of Mj garnet is predicted to exist in this area, causing both the appearance of an intra-MTZ LVL and a double 660 discontinuity. Zones of upwelling, even if shallower and only affecting the 410, continue to occur to the south of the Gibraltar-Alboran slab and possibly along the Atlas range. The upwelling in NW Maghreb and the areas of depressed 410 in Iberia and SE France correlate well with active anorogenic volcanism. The existence of LVL atop the 410 in these locations seems to further suggest a link between a water-enriched MTZ and the regional intraplate magmatism. Finally, we found that deep-focus seismicity beneath Granada clusters in an area where the 660 starts to deepen near the transition from the back of the cold Gibraltar-Alboran slab to the upwelling zone in the Gulf of Cadiz.

CRedit authorship contribution statement

J.A. Parera-Portell: Writing – original draft, Investigation, Formal analysis. **F.d.L. Mancilla:** Writing – review & editing, Investigation, Conceptualization. **J. Morales:** Writing – review & editing, Investigation. **J. Díaz:** Writing – review & editing, Resources.

Declaration of competing interest

No conflict of interest exists.

Data availability

Data from open seismic networks can be accessed through the ORFEUS EIDA and FDSN data services. Access to data from restricted networks is subject to authorization by the Principal Investigators.

Acknowledgments

This work has been funded by the grant PID2019-109608GB-I00 from the Spanish Research Agency MCIN/AEI/10.13039/501100011033, and the FPI grant PRE2020-092556 from the Spanish Research Agency MCIN/AEI/10.13039/501100011033 and the European Social Fund.

We want to acknowledge all the teams involved in the design, installation and maintenance of the permanent and temporary seismic networks, which provided the essential data to carry out this

study (2M, 3D, 3 J, 8A, 9C, 9H, CA, ES, FR, GE, Andalusian Seismic Network, IB, IU, LC, LX, MN, PINSAPO, PM, RD, SC, TAPAS, TROPICAL, WM, X7, XB, YR, YS, ZC, ZI and ZU). We thank ORFEUS EIDA (<http://www.orfeus-eu.org/data/eida/>) and FDSN (<https://www.fdsn.org/services/>) data services for providing easy access to seismic data. We want to thank the Principal Investigators of the temporary seismic networks with restricted access for making available their data. This work has benefited from the infrastructure of the GEO3BCN-CSIC LabSis laboratory (<http://labsis.geo3bcn.csic.es>). We also thank Maximiliano Bezada, Mickaël Bonnín and Antonio Villaseñor for sharing the regional tomographic models and all people involved in making global models UUP-07 and DETOX-P3 available and ready for visualization in SubMachine (<https://www.earth.ox.ac.uk/~smachine/>). We acknowledge use of the following software: SAC (Goldstein and Snoke, 2005), ObsPy (Krischer et al., 2015) and GMT (Wessel et al., 2019).

Appendix A. Supplementary material

Supplementary material related to this article can be found online at <https://doi.org/10.1016/j.epsl.2024.118798>.

References

- Amaru, M., 2007. Global Travel Time Tomography with 3-D Reference Models. Ph.D. thesis. University of Utrecht.
- Bercovici, D., Karato, S.I., 2003. Whole-mantle convection and the transition-zone water filter. *Nature* 425, 39–44. <https://doi.org/10.1038/nature01918>.
- Bezada, M., Humphreys, E., Toomey, D., Harnafi, M., Dávila, J., Gallart, J., 2013. Evidence for slab rollback in westernmost Mediterranean from improved upper mantle imaging. *Earth Planet. Sci. Lett.* 368, 51–60. <https://doi.org/10.1016/j.epsl.2013.02.024>.
- Bonato, L., Schimmel, M., Gallart, J., Morales, J., 2015. The upper-mantle transition zone beneath the Ibero-Maghreb region as seen by teleseismic Pds phases. *Tectonophysics* 663, 212–224. <https://doi.org/10.1016/j.tecto.2015.02.002>.
- Bonnin, M., Nolet, G., Villaseñor, A., Gallart, J., Thomas, C., 2014. Multiple-frequency tomography of the upper mantle beneath the African/Iberian collision zone. *Geophys. J. Int.* 198, 1458–1473. <https://doi.org/10.1093/gji/ggu214>.
- Carminati, E., Lustrino, M., Doglioni, C., 2012. Geodynamic evolution of the central and western Mediterranean: tectonics vs. igneous petrology constraints. *Tectonophysics* 579, 173–192. <https://doi.org/10.1016/j.tecto.2012.01.026>.
- Civiero, C., Custódio, S., Duarte, J.C., Mendes, V.B., Faccenna, C., 2020. Dynamics of the Gibraltar Arc system: a complex interaction between plate convergence, slab pull, and mantle flow. *J. Geophys. Res., Solid Earth* 125. <https://doi.org/10.1029/2019jb018873>.
- Civiero, C., Custódio, S., Rawlinson, N., Strak, V., Silveira, G., Arroucau, P., Corela, C., 2019. Thermal nature of mantle upwellings below the Ibero-Western Maghreb region inferred from teleseismic tomography. *J. Geophys. Res., Solid Earth* 124, 1781–1801. <https://doi.org/10.1029/2018jb016531>.
- Civiero, C., Strak, V., Custódio, S., Silveira, G., Rawlinson, N., Arroucau, P., Corela, C., 2018. A common deep source for upper-mantle upwellings below the Ibero-Western Maghreb region from teleseismic P-wave travel-time tomography. *Earth Planet. Sci. Lett.* 499, 157–172. <https://doi.org/10.1016/j.epsl.2018.07.024>.
- Collier, J.D., Helffrich, G.R., 1997. Topography of the “410” and “660” km seismic discontinuities in the Izu-Bonin subduction zone. *Geophys. Res. Lett.* 24, 1535–1538. <https://doi.org/10.1029/97gl01383>.
- Diaz, J., Gallart, J., Villaseñor, A., Mancilla, F., Pazos, A., Córdoba, D., Pulgar, J.A., Ibarra, P., Harnafi, M., 2010. Mantle dynamics beneath the Gibraltar Arc (western Mediterranean) from shear-wave splitting measurements on a dense seismic array. *Geophys. Res. Lett.* 37. <https://doi.org/10.1029/2010gl044201>.
- Diaz, J., Torne, M., Vergés, J., Jiménez-Munt, I., Martí, J., Carbonell, R., Schimmel, M., Geyer, A., Ruiz, M., García-Castellanos, D., Alvarez-Marrón, J., Brown, D., Villaseñor, A., Ayala, C., Palomeras, I., Fernandez, M., Gallart, J., 2021. Four decades of geophysical research on Iberia and adjacent margins. *Earth-Sci. Rev.* 222, 103841. <https://doi.org/10.1016/j.earscirev.2021.103841>.
- Faccenna, C., Becker, T.W., Auer, L., Billi, A., Boschi, L., Brun, J.P., Capitanio, F.A., Funiello, F., Horvath, F., Jolivet, L., Píromallo, C., Royden, L., Rossetti, F., Serpelloni, E., 2014. Mantle dynamics in the Mediterranean. *Rev. Geophys.* 52, 283–332. <https://doi.org/10.1002/2013rg000444>.
- Faccenna, C., Píromallo, C., Crespo-Blanc, A., Jolivet, L., Rossetti, F., 2004. Lateral slab deformation and the origin of the western Mediterranean arcs. *Tectonics* 23. <https://doi.org/10.1029/2002tc001488>.
- Frassetto, A., Zandt, G., Gilbert, H., Owens, T.J., Jones, C.H., 2010. Improved imaging with phase-weighted common conversion point stacks of receiver functions. *Geophys. J. Int.* <https://doi.org/10.1111/j.1365-246x.2010.04617.x>.
- Freitas, D., Manthilake, G., Schiavi, F., Chantel, J., Bolfan-Casanova, N., Bouhifd, M.A., Andraut, D., 2017. Experimental evidence supporting a global melt layer at the base of the Earth’s upper mantle. *Nat. Commun.* 8. <https://doi.org/10.1038/s41467-017-02275-9>.
- Goldstein, P., Snoke, A., 2005. SAC availability for the IRIS community. *Incorp. Res. Inst. Seismol. Newslett.* 7.
- Han, G., Li, J., Guo, G., Mooney, W.D., Karato, S.I., Yuen, D.A., 2021. Pervasive low-velocity layer atop the 410-km discontinuity beneath the northwest Pacific subduction zone: implications for rheology and geodynamics. *Earth Planet. Sci. Lett.* 554, 116642. <https://doi.org/10.1016/j.epsl.2020.116642>.
- Handy, M.R., Schmid, S.M., Paffrath, M., Friederich, W., 2021. Orogenic lithosphere and slabs in the greater Alpine area – interpretations based on teleseismic P-wave tomography. *Solid Earth* 12, 2633–2669. <https://doi.org/10.5194/se-12-2633-2021>.
- Hosseini, K., Matthews, K.J., Sigloch, K., Shepherd, G.E., Domeier, M., Tsekhmistrenko, M., 2018. SubMachine: web-based tools for exploring seismic tomography and other models of Earth’s deep interior. *Geochem. Geophys. Geosyst.* 19, 1464–1483. <https://doi.org/10.1029/2018gc007431>.
- Hosseini, K., Sigloch, K., Tsekhmistrenko, M., Zaheri, A., Nissen-Meyer, T., Igel, H., 2019. Global mantle structure from multifrequency tomography using P, PP and P-diffracted waves. *Geophys. J. Int.* 220, 96–141. <https://doi.org/10.1093/gji/ggz394>.
- van Keken, P.E., Hacker, B.R., Syracuse, E.M., Abers, G.A., 2011. Subduction factory: 4. depth-dependent flux of H₂O from subducting slabs worldwide. *J. Geophys. Res.* 116. <https://doi.org/10.1029/2010jb007922>.
- Krischer, L., Megies, T., Barsch, R., Beyreuther, M., Lecocq, T., Caudron, C., Wassermann, J., 2015. ObsPy: a bridge for seismology into the scientific Python ecosystem. *Comput. Sci. Discov.* 8, 014003. <https://doi.org/10.1088/1749-4699/8/1/014003>.
- Langston, C.A., 1979. Structure under Mount Rainier, Washington, inferred from teleseismic body waves. *J. Geophys. Res.* 84, 4749. <https://doi.org/10.1029/jb084ib09p04749>.
- Leahy, G.M., Bercovici, D., 2007. On the dynamics of a hydrous melt layer above the transition zone. *J. Geophys. Res., Solid Earth* 112. <https://doi.org/10.1029/2006jb004631>.
- Lee, H., Bezada, M.J., Kim, Y., 2022. The origin of the low-velocity anomalies beneath the rootless Atlas Mountains: insights gained from modeling of anisotropy developed by the travel of Canary Plume. *J. Geophys. Res., Solid Earth* 127. <https://doi.org/10.1029/2022jb024622>.
- Ligorria, J., Ammon, C., 1999. Iterative deconvolution and receiver-function estimation. *Bull. Seismol. Soc. Am.* 89, 1395–1400.
- Litasov, K.D., Ohtani, E., 2007. Effect of Water on the Phase Relations in Earth’s Mantle and Deep Water Cycle. *Geological Society of America*, pp. 115–156.
- Litasov, K.D., Ohtani, E., Sano, A., Suzuki, A., Funakoshi, K., 2005. Wet subduction versus cold subduction. *Geophys. Res. Lett.* 32. <https://doi.org/10.1029/2005gl022921>.
- Mancilla, F.d.L., Heit, B., Morales, J., Yuan, X., Stich, D., Molina-Aguilera, A., Azañón, J.M., Martín, R., 2018. A STEP fault in Central Betics, associated with lateral lithospheric tearing at the northern edge of the Gibraltar arc subduction system. *Earth Planet. Sci. Lett.* 486, 32–40. <https://doi.org/10.1016/j.epsl.2018.01.008>.
- Miller, M.S., Becker, T.W., 2013. Reactivated lithospheric-scale discontinuities localize dynamic uplift of the Moroccan Atlas Mountains. *Geology* 42, 35–38. <https://doi.org/10.1130/g34959.1>.
- Mitas, L., Mitasova, H., 1999. Spatial Interpolation. In: *Geographical Information Systems: Principles, Techniques, Management and Applications*. Wiley, pp. 481–492.
- Nagel, T.J., Dueterhoeft, E., Schiffer, C., 2018. Garnet-controlled very low velocities in the lower mantle transition zone at sites of mantle upwelling. *Terra Nova* 30, 333–340. <https://doi.org/10.1111/ter.12348>.
- Schmandt, B., Jacobsen, S.D., Becker, T.W., Liu, Z., Dueker, K.G., 2014. Dehydration melting at the top of the lower mantle. *Science* 344, 1265–1268. <https://doi.org/10.1126/science.1253358>.
- Schmerr, N., Garnero, E.J., 2007. Upper mantle discontinuity topography from thermal and chemical heterogeneity. *Science* 318, 623–626. <https://doi.org/10.1126/science.1145962>.
- Serpelloni, E., Vannucci, G., Pondrelli, S., Argnani, A., Casula, G., Anzidei, M., Baldi, P., Gasperini, P., 2007. Kinematics of the western Africa-Eurasia plate boundary from focal mechanisms and GPS data. *Geophys. J. Int.* 169, 1180–1200. <https://doi.org/10.1111/j.1365-246x.2007.03367.x>.
- Shen, X., Yuan, X., Li, X., 2014. A ubiquitous low-velocity layer at the base of the mantle transition zone. *Geophys. Res. Lett.* 41, 836–842. <https://doi.org/10.1002/2013gl058918>.
- Spakman, W., Wortel, R., 2004. *A Tomographic View on Western Mediterranean Geodynamics*. Springer, Berlin Heidelberg, pp. 31–52.
- Stich, D., Serpelloni, E., de Lis Mancilla, F., Morales, J., 2006. Kinematics of the Iberia-Maghreb plate contact from seismic moment tensors and GPS observations. *Tectonophysics* 426, 295–317. <https://doi.org/10.1016/j.tecto.2006.08.004>.
- Sun, D., Miller, M.S., 2024. Revealing the secrets of the Western Mediterranean: a deep earthquake and the overturned slab. *Seism. Rec.* 4, 52–61. <https://doi.org/10.1785/0320230049>.
- Sun, D., Miller, M.S., Holt, A.F., Becker, T.W., 2014. Hot upwelling conduit beneath the Atlas mountains, Morocco. *Geophys. Res. Lett.* 41, 8037–8044. <https://doi.org/10.1002/2014gl061884>.
- Sun, M., Liu, K.H., Fu, X., Gao, S.S., 2017. Receiver function imaging of mantle transition zone discontinuities beneath the Tanzania Craton and adjacent segments of the East African rift system. *Geophys. Res. Lett.* 44. <https://doi.org/10.1002/2017gl075485>.

- Tauzin, B., van der Hilst, R.D., Wittlinger, G., Ricard, Y., 2013. Multiple transition zone seismic discontinuities and low velocity layers below western United States. *J. Geophys. Res., Solid Earth* 118, 2307–2322. <https://doi.org/10.1002/jgrb.50182>.
- Tauzin, B., Kim, S., Kennett, B., 2017. Pervasive seismic low-velocity zones within stagnant plates in the mantle transition zone: thermal or compositional origin? *Earth Planet. Sci. Lett.* 477, 1–13. <https://doi.org/10.1016/j.epsl.2017.08.006>.
- Tauzin, B., Ricard, Y., 2014. Seismically deduced thermodynamics phase diagrams for the mantle transition zone. *Earth Planet. Sci. Lett.* 401, 337–346. <https://doi.org/10.1016/j.epsl.2014.05.039>.
- Villaseñor, A., Chevrot, S., Harnafi, M., Gallart, J., Pazos, A., Serrano, I., Córdoba, D., Pulgar, J.A., Ibarra, P., 2015. Subduction and volcanism in the Iberia–North Africa collision zone from tomographic images of the upper mantle. *Tectonophysics* 663, 238–249. <https://doi.org/10.1016/j.tecto.2015.08.042>.
- Vinnik, L., 1977. Detection of waves converted from P to SV in the mantle. *Phys. Earth Planet. Inter.* 15, 39–45. [https://doi.org/10.1016/0031-9201\(77\)90008-5](https://doi.org/10.1016/0031-9201(77)90008-5).
- Wang, X., Chen, Q.F., Niu, F., Wei, S., Ning, J., Li, J., Wang, W., Buchen, J., Liu, L., 2020. Distinct slab interfaces imaged within the mantle transition zone. *Nat. Geosci.* 13, 822–827. <https://doi.org/10.1038/s41561-020-00653-5>.
- Waszek, L., Tauzin, B., Schmerr, N.C., Ballmer, M.D., Afonso, J.C., 2021. A poorly mixed mantle transition zone and its thermal state inferred from seismic waves. *Nat. Geosci.* 14, 949–955. <https://doi.org/10.1038/s41561-021-00850-w>.
- Wessel, P., Luis, J.F., Uieda, L., Scharroo, R., Wobbe, F., Smith, W.H.F., Tian, D., 2019. The generic mapping tools version 6. *Geochem. Geophys. Geosyst.* 20, 5556–5564. <https://doi.org/10.1029/2019gc008515>.
- Yang, J., Faccenda, M., 2020. Intraplate volcanism originating from upwelling hydrous mantle transition zone. *Nature* 579, 88–91. <https://doi.org/10.1038/s41586-020-2045-y>.
- Yuan, X., Sobolev, S., Kind, R., Oncken, O., Bock, G., Asch, G., Schurr, B., Graeber, F., Rudloff, A., Hanka, W., Wylegalla, K., Tibi, R., Haberland, G., Rietbrock, A., Giese, P., Wigger, P., Röwer, P., Zandt, G., Beck, S., Wallace, T., Pardo, M., Comte, D., 2000. Subduction and collision processes in the central Andes constrained by converted seismic phases. *Nature* 408, 958–961. <https://doi.org/10.1038/35050073>.